


# Charge-state independent anomalous transport for a wide range of different impurity species observed at Wendelstein 7-X


Cite as: Phys. Plasmas **27**, 052510 (2020); <https://doi.org/10.1063/5.0004462>

Submitted: 12 February 2020 • Accepted: 21 April 2020 • Published Online: 29 May 2020

 A. Langenberg,  Th. Wegner,  N. A. Pablant, et al.

## COLLECTIONS

 This paper was selected as Featured

 This paper was selected as Scilight



View Online



Export Citation



CrossMark

## ARTICLES YOU MAY BE INTERESTED IN

[Performance of Wendelstein 7-X stellarator plasmas during the first divertor operation phase](#)  
Physics of Plasmas **26**, 082504 (2019); <https://doi.org/10.1063/1.5098761>

[Charge exchange recombination spectroscopy at Wendelstein 7-X](#)  
Review of Scientific Instruments **91**, 023507 (2020); <https://doi.org/10.1063/1.5132936>

[Stellarator impurity transport experiments show a favorable anomalous transport mechanism](#)  
Scilight **2020**, 221108 (2020); <https://doi.org/10.1063/10.0001355>



Physics of Plasmas  
Features in Plasma Physics Webinars

Register Today!



# Charge-state independent anomalous transport for a wide range of different impurity species observed at Wendelstein 7-X

Cite as: Phys. Plasmas **27**, 052510 (2020); doi: 10.1063/5.0004462

Submitted: 12 February 2020 · Accepted: 21 April 2020 ·

Published Online: 29 May 2020




View Online



Export Citation



CrossMark

A. Langenberg,<sup>1,a)</sup>  Th. Wegner,<sup>1</sup>  N. A. Pablant,<sup>2</sup>  O. Marchuk,<sup>3</sup>  B. Geiger,<sup>1</sup> N. Tamura,<sup>4</sup>  R. Bussiahn,<sup>1</sup>  M. Kubkowska,<sup>5</sup>  A. Mollén,<sup>2</sup> P. Traverso,<sup>2</sup> H. M. Smith,<sup>1</sup> G. Fuchert,<sup>1</sup> S. Bozhnikov,<sup>1</sup>  H. Damm,<sup>1</sup>  E. Pasch,<sup>1</sup> K.-J. Brunner,<sup>1</sup>  J. Knauer,<sup>1</sup>  M. Beurskens,<sup>1</sup> R. Burhenn,<sup>1</sup> R. C. Wolf,<sup>1</sup>  and W7-X Team<sup>b)</sup>

## AFFILIATIONS

<sup>1</sup>Max-Planck-Institut für Plasmaphysik, 17491 Greifswald, Germany

<sup>2</sup>Princeton Plasma Physics Laboratory, Princeton, New Jersey 08543, USA

<sup>3</sup>Institut für Energie- und Klimaforschung, Forschungszentrum Jülich GmbH, 52425 Jülich, Germany

<sup>4</sup>National Institute for Fusion Science, Gifu 509-5292, Japan

<sup>5</sup>Institute of Plasma Physics and Laser Microfusion, 01-497 Warsaw, Poland

<sup>a)</sup>Author to whom correspondence should be addressed: [andreas.langenberg@ipp.mpg.de](mailto:andreas.langenberg@ipp.mpg.de)

<sup>b)</sup>T. Klinger *et al.*, Nucl. Fusion **59**, 112004 (2019).

## ABSTRACT

In this paper, the plasma volume averaged impurity confinement of selected charge states and impurity species has been characterized for the Stellarator Wendelstein 7-X (W7-X), covering a wide range of atomic charges ( $Z = 12-44$ ) and atomic masses ( $M = 28-184$ ). A comparison of the experimental findings to theoretical neoclassical and turbulent transport expectations suggests, aside from/in addition to the neoclassical transport, an additional significant anomalous transport mechanism, which is not inconsistent with the predictions of a turbulence dominated impurity transport and is in agreement with the experimental results from recent transport studies based on the direct measurements of impurity diffusion profiles, performed at W7-X.

© 2020 Author(s). All article content, except where otherwise noted, is licensed under a Creative Commons Attribution (CC BY) license (<http://creativecommons.org/licenses/by/4.0/>). <https://doi.org/10.1063/5.0004462>

## I. INTRODUCTION

The presence of impurities in the plasma can have a significant impact on the overall plasma properties, including the aspects of improved but also of degraded plasma performance. Typical examples are power exhaust<sup>1,2</sup> or edge localized modes buffering<sup>3</sup> by impurity seeding, on the one hand, but also, e.g., undesired plasma termination events,<sup>4,5</sup> on the other hand. In the latter case, particular high  $Z$  materials may cause radiative collapses due to dissipative radiative transitions of non-fully ionized impurities, especially critical in combination with impurity accumulation scenarios.<sup>5,6</sup> As the divertor and other plasma facing components, being the main edge impurity sources in fusion devices, are designed using low as well as high  $Z$  materials like C,<sup>7</sup> Fe,<sup>8</sup> or W,<sup>9</sup> a comparative experimental determination of the transport properties of different impurity species from low to high  $Z$  materials is of general interest. The first experimental works on this topic in low confinement scenarios of Tokamaks<sup>10-14</sup> and Stellarators<sup>15</sup> did

not observe a significant variation of the impurity confinement with  $Z$ , using, however, quite a limited number of different materials.

Theoretical expectations for the impurity transport of different impurity species and impurity charges predict either a pronounced variation of the convective transport with  $Z$  or rather the unaffected transport properties, depending on the, respectively, dominant transport mechanism, namely neoclassical<sup>16,17</sup> or turbulent transport.<sup>18</sup> Moreover, in non-axis-symmetric devices, additional aspects as the existence of a mixed collisionality regime<sup>19</sup> or the buildup of a radial electric field<sup>20,21</sup> are predicted by the neoclassical theory and are expected to have an impact on the impurity transport.

In this study, impurity transport properties have been investigated for a wide range of different impurity species within a stationary plasma scenario by measuring the impurity transport times  $\tau_I$ <sup>22,23</sup> after pulsed impurity injections. After an introduction of the experimental method (Sec. II), experimentally observed transport properties are

discussed comparatively to theoretical expectations with respect to the neoclassical and turbulent transport (Sec. III).

## II. EXPERIMENTAL METHOD

The Stellarator W7-X is a magnetic confinement fusion device, designed for a steady state plasma operation of up to 30 min under fusion relevant plasma conditions, including neoclassical optimized particle confinement, minimized bootstrap currents, and high beta values.<sup>24</sup> For an experimental determination of the global transport properties in W7-X, trace amounts of several different, non-recycling impurity species have been injected into stationary plasmas of constant heating power, temperature, and electron density. The injection of impurities has been realized using a laser blow-off (LBO) system<sup>22</sup> with a total amount of injected particles of less than  $1 \times 10^{18}$  particles, as estimated by Wegner *et al.*<sup>22</sup> being non-perturbative to the plasma temperature and density profiles. The signals of the highly ionized impurities, located well inside the bulk plasma, have been recorded making use of the high resolution X-ray imaging spectrometer (HR-XIS) and the X-ray imaging crystal spectrometer (XICS),<sup>15</sup> where XICS is used to measure  $T_i$  and  $E_r$  monitoring Ar impurities and HR-XIS is used to measure the injected impurity signals other than Ar. Alternatively, the X-ray radiation from the injected impurities can also be observed by the pulse height analysis system (PHA), but with a lower temporal resolution.<sup>25</sup> For each impurity species, identical plasma parameters have been reproduced and a separate experimental program was used for each impurity species. All data shown in this work have been taken during the third experimental campaign of W7-X (OP1.2b)<sup>26</sup> in the magnetic standard configuration.<sup>27</sup> Plasma parameters have been chosen to obtain plasmas in the central electron root confinement (CERC) scenario, representing the majority of experimental programs from OP1.2b.

In Fig. 1, the measured temperature and density profiles of the repeated experiment programs are shown. As a consequence of the low electron density ( $n_e = 3.2 \times 10^{19} \text{ m}^{-3}$ ) and a pure electron heating using electron cyclotron resonance heating (ECRH),<sup>28</sup> all experiment programs in this study have been performed in the CERC conditions with central  $T_e$  values being significantly larger than  $T_i$  [see Fig. 1(a)], and a positive radial electric field  $E_r$  in the plasma center as measured by XICS in agreement with the neoclassical predictions,<sup>20</sup> see the symbols and the solid line in Fig. 1(b).

Figure 2 shows an overview of the measured impurity signal time traces for all impurity species investigated in this study. Right after the injection, the impurity brightness shows a fast rise followed by an exponential decay. A fit of the exponentially decaying impurity signal (shaded time interval in Fig. 2) yields the impurity transport time  $\tau_I$  being a direct measure of the global impurity confinement, as discussed in detail elsewhere.<sup>22,23</sup> Since the HR-XIS and XICS data are functions of both time and plasma radius  $\rho$ , defined as the square root of the normalized toroidal magnetic flux, in this study, the  $\rho$  dependence of the impurity signal has been omitted by summing the detector counts over all viewing chords. For simulations of the impurity transport, the modeled signals shown in Figs. 4(c) and 4(d) have been derived from the volume integral of the calculated impurity densities. This reduction of the experimental and theoretical data over  $\rho$  is well justified as impurity density profile shapes are expected to become stationary after a typical equilibration time<sup>29</sup> that for W7-X is on the order of 100 ms, as shown in Refs. 15 and 22.

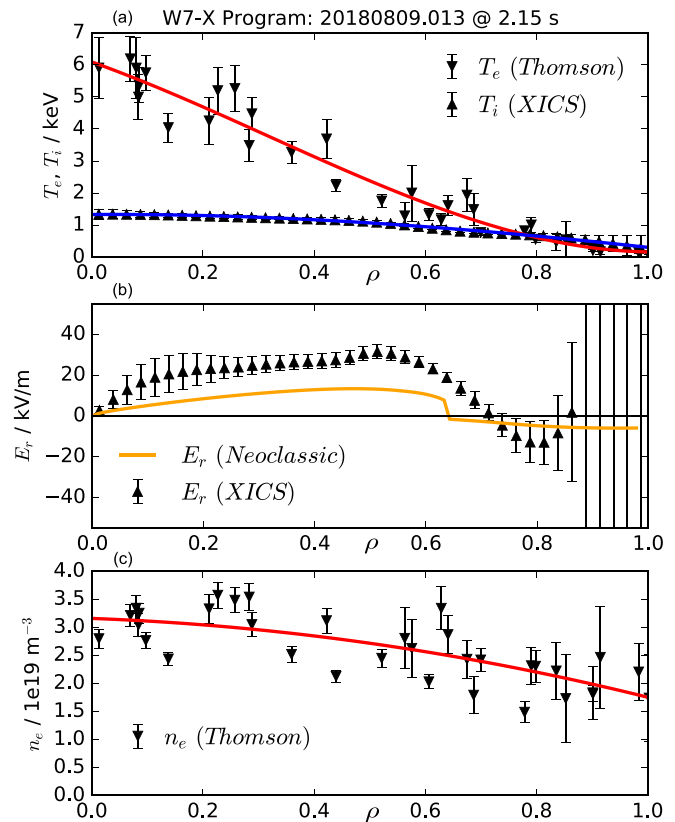


FIG. 1. (a) Temperature, (b) radial electric field, and (c) density profiles as measured by the Thomson scattering (triangles down) and the XICS diagnostics (triangles up). Solid lines are fitted profiles, used as input for transport code calculations (see Sec. IV).

## III. RESULTS AND DISCUSSION

### A. Global confinement for different impurity species

In Fig. 3, the experimentally derived impurity transport times  $\tau_I$  for numerous impurities, namely silicon, titanium, iron, nickel, copper, molybdenum, and tungsten, are shown. As can be seen, the measured  $\tau_I$  values are very similar for a wide range of different impurities under the variation of the atomic number  $A$  as well as the atomic charge  $Z$  and the charge to mass ratio  $Z/M$ . In particular, although the impurity charge varies by about  $\Delta Z = 55\%$  going from  $\text{Ti}^{20+}$  to  $\text{W}^{44+}$ , the observed change in  $\tau_I$  is only of  $\Delta\tau_I = 6\% \pm 2\%$ . This shows at most a very weak dependence of impurity confinement for both the impurity charge and the impurity mass. This trend has also been observed in earlier studies at Alcator C-mod<sup>10</sup> and W7-X,<sup>15</sup> although in those cases, the limited number of impurity species did not allow to draw any general conclusions on the  $Z$  and  $M$  dependences of impurity confinement so far.

It should be mentioned that, despite the edge deposition of impurities using LBO, the injected impurities penetrate deep into the plasma core<sup>30,31</sup> and the observed  $\tau_I$  values represent the bulk plasma properties and are not restricted to the plasma edge. This statement is supported by the initial results from impurities deposited close to the plasma center using the TESPEL injection system,<sup>32</sup> where also a

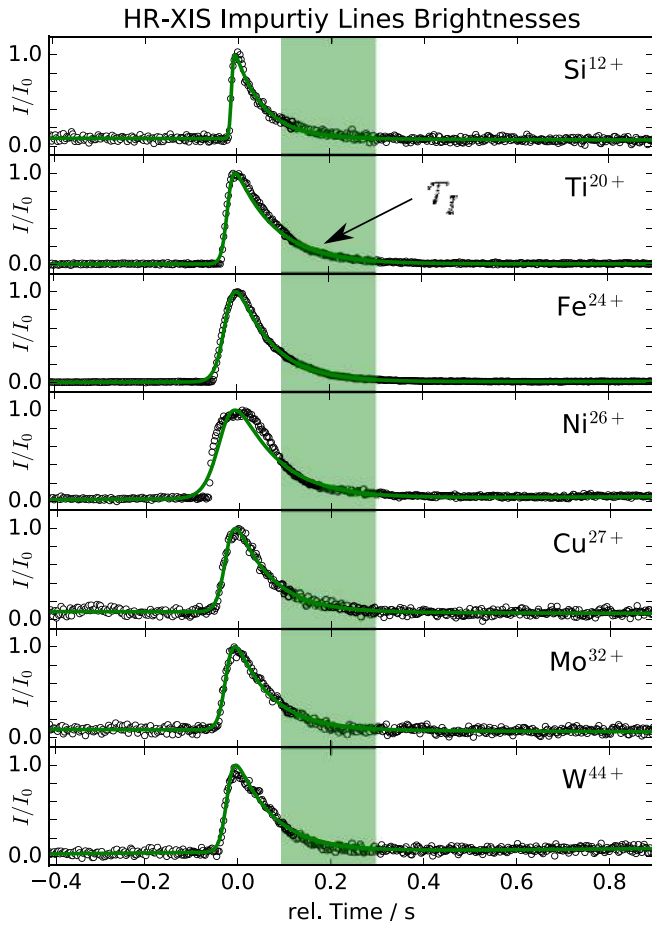


**FIG. 2.** Time traces for the brightness of several impurity species after pulsed impurity injections. The solid line corresponds to a fit of measured data (symbols), and the shaded area was used for the  $\tau_I$  determination.

similar trend of the above discussed weak  $Z$  and  $M$  dependences of  $\tau_I$  has been observed.<sup>33</sup>

### B. Theoretical expectations for impurity transport

In this section, theoretical predictions for the neoclassical (including classical) impurity transport, on the one hand, and turbulence

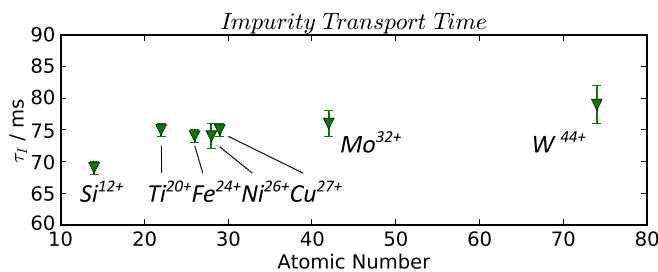


**FIG. 3.** Experimentally obtained impurity transport times  $\tau_I$  for various atomic numbers of different atomic charges and charge to mass ratios of the impurity species.

driven transport, on the other hand, are discussed comparatively and with respect to the experimental findings.

Models of the neoclassical transport in the high collisionality regime ( $\nu^* \gg 10^{-2}$ , relevant to our experimental conditions) of highly charged impurities predict a pronounced  $Z$  dependence of the impurity convection velocity  $v$  and a charge and mass independent impurity diffusion  $D$ ,<sup>16,17,19</sup> with the former effect having a direct impact on the transport times  $\tau_I$

$$\nu^* \gg 10^{-2} \Rightarrow D = const., \quad v \propto Z \cdot E_r. \quad (1)$$

Here, the collisionality  $\nu^*$  is defined according to<sup>17</sup> as

$$\nu^* = R_0 \nu_c / (\bar{v}), \quad (2)$$

with the torus major radius  $R_0$ , the rotational transform on the magnetic axis  $\iota$ , the particle speed  $\bar{v}$ , and the collision frequency  $\nu_c$

$$\nu_c \propto \frac{n_e Z^2}{4\pi(\epsilon_0 M)^2}. \quad (3)$$

In order to show the neoclassical expected  $\tau_I$  to  $Z$  dependence explicitly for the experimental plasma conditions of this study,  $\tau_I$  has been modeled using the one dimensional (magnetic flux surface averaged) transport code STRAHL.<sup>34</sup> As input parameters, the experimentally obtained  $T_e$ ,  $T_i$ , and  $n_e$  profiles (solid lines in Fig. 1) as well as the neoclassical expected  $E_r$  and the diffusive  $D$  and convective  $v$  transport parameter profiles, derived from the drift kinetic equation solver code DKES,<sup>35,36</sup> have been used in the STRAHL modeling.

As the collision operator implemented in DKES is generally not valid at high collisionalities but the code is significantly cheaper with respect to the computational time, the obtained DKES results have been cross validated exemplarily for  $\text{Si}^{12+}$  and  $\text{W}^{44+}$  impurities using the continuum drift-kinetic solver SFINCS,<sup>37–39</sup> which implements the full linearized Fokker–Planck–Landau operator. As evident from Figs. 4(a) and 4(b), the DKES results for the  $D$  and  $v$  profiles (solid lines) compare reasonably well with the calculated SFINCS profiles shown as dashed lines. Therefore, throughout this work, the DKES results have been used as STRAHL input parameters for the  $\text{Si}^{12+}$ ,  $\text{Ti}^{20+}$ ,  $\text{Fe}^{24+}$ ,  $\text{Ni}^{26+}$ ,  $\text{Cu}^{27+}$ ,  $\text{Mo}^{32+}$ , and  $\text{W}^{44+}$  elements, considering the classical as well as the neoclassical transport.

The  $D$  profile shapes [Fig. 4(a)] are rather broad with a step-like reduction at the radial position of the crossover of  $E_r$  from the positive (electron root) to negative (ion-root) values; see Fig. 1(b). Also, the  $v$  profiles [Fig. 4(b)] exhibit a similar reduction at the  $E_r$  crossover, both effects also observed in other neoclassical transport studies<sup>40,41</sup> and in agreement with the shown profiles using SFINCS. We note that the neoclassical particle fluxes induced by the low  $D$  values are significantly smaller than those induced by  $v$ , i.e., the logarithmic impurity density gradient  $d(\ln(n_z))/dr$  must be of order 100 or larger for the diffusive transport to compare to the convective transport. At high collisionality, the neoclassical convection is not necessarily dominated by the radial electric field, and a lower  $Z$  impurity could experience a stronger convection than a higher  $Z$  impurity as seen in the plasma center. At the plasma edge, the  $v$  profiles exhibit higher positive (outward directed) convection velocities with higher  $Z$ , as expected from Eq. (1). The convective transport is determined by an interplay between the temperature screening and the drive from the main ion density gradient, as well as the relative size of the classical and neoclassical channels.

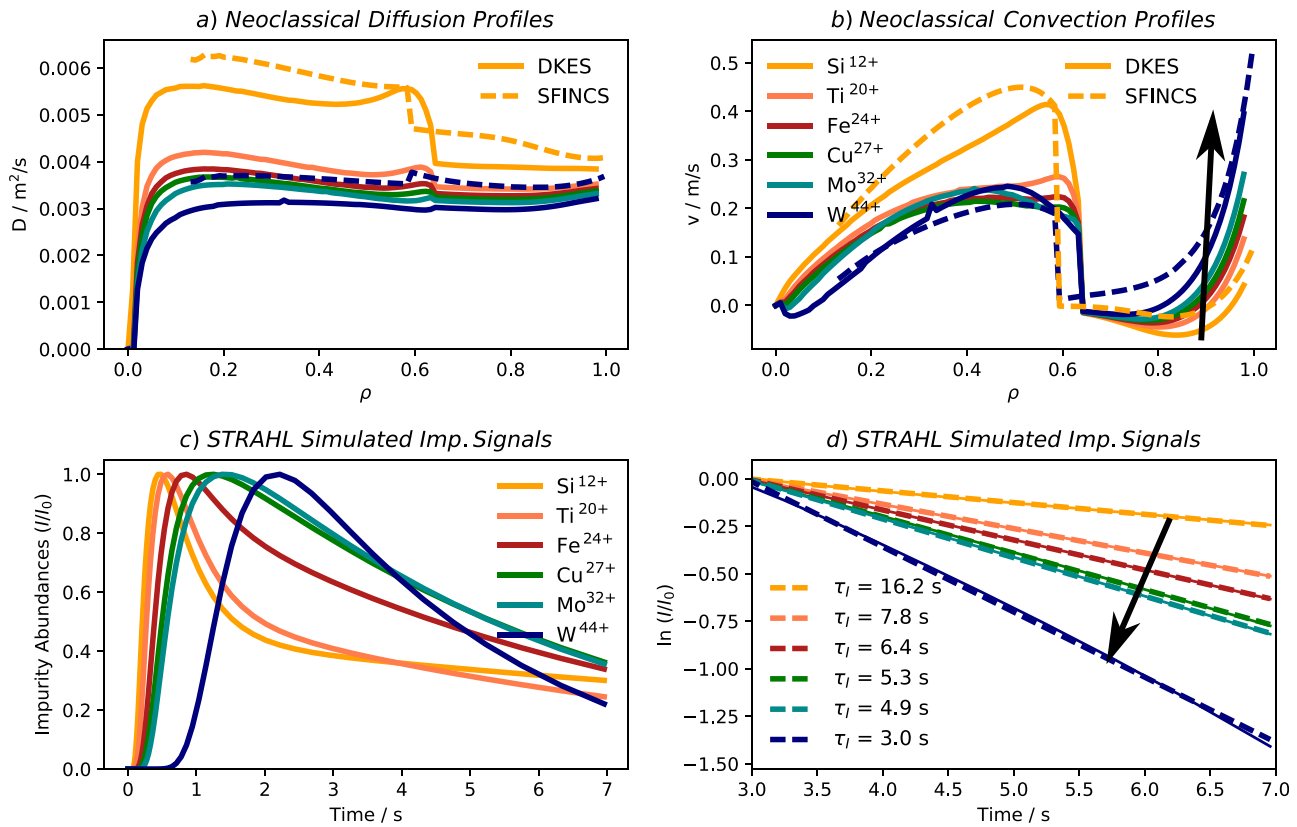


**FIG. 4.** (a) and (b) Neoclassical (including classical) expected  $D$  and  $v$  profiles for different impurity species shown in Fig. 1 for a CERC plasma scenario. (c) and (d) Normalized STRAHL simulated time traces of different impurity species in a linear (c) and a logarithmic scale (d), together with modeled impurity transport times  $\tau_I$ .

The modeled  $D$  and  $v$  profiles cause weaker confinement and shorter transport times  $\tau_I$  of the high  $Z$  materials, evident from the STRAHL simulated time traces of the impurity signals shown in Figs. 4(c) and 4(d). Arrows on Fig. 4 indicate the theoretical expected increasing  $v$  and decreasing  $\tau_I$  with rising  $Z$ , as discussed above.

In Fig. 5, the modeled  $\tau_I$  values (dots) are shown together with those experimentally derived (triangles) for the different impurity

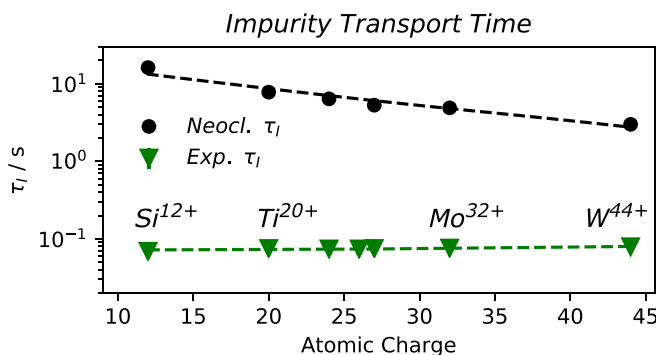


**FIG. 5.** Comparison of the neoclassical expected and experimentally observed impurity transport times  $\tau_I$  along  $Z$  for the impurity species shown in Fig. 3.

species on a logarithmic scale. As can be seen, the experimental transport times do not follow the neoclassical expected trend of the reduced confinement of higher  $Z$  materials, comparing the dashed lines in Fig. 5. Even more striking, the experimental  $\tau_I$  values undercut the theoretical ones up to a factor of about 100 in the case of Ti<sup>20+</sup>. Both observations are in line with the recent observations of large experimental diffusivities for Ar and Fe impurities in W7-X plasmas,<sup>30,40</sup> hinting at a significant non-neoclassical impurity transport mechanism.

In fact, the observed marginal effect of the impurity mass and charge state on the transport properties of highly charged impurities is in agreement with the theoretical predictions when the impurity transport is dominated by turbulent diffusion.<sup>18</sup> In that case, a gyrokinetic model of quasilinear impurity transport yields a diffusion transport parameter  $D$  being independent of  $Z$  and  $M$  and which is dominant over the convective transport  $v$ . This predicted independence of  $D$  over  $Z$  and  $M$  is in line with the experimental observations shown in Figs. 3 and 5: here,  $\tau_I$  is almost constant within the experimental uncertainties, despite a significant variation of  $Z = (12^+ - 44^+)$  as well as  $Z/M = (0.23 - 0.45)$ .

#### IV. SUMMARY AND CONCLUSIONS

The experimental finding of a weak  $M$  and  $Z$  dependence of the transport time of highly charged impurities, theory,<sup>18</sup> and direct measurements of impurity diffusion profiles<sup>30,40</sup> suggests that the impurity

transport in W7-X is dominated by the anomalous transport, being not inconsistent with the theoretical expectations of turbulent transport.<sup>18,42</sup> The combination of weak  $Z$  dependence and high diffusivities is beneficial for avoiding impurity accumulation in long pulse operations of W7-X, especially for the high  $Z$  materials, including tungsten.

So far, the  $Z$  dependence on impurity transport was systematically studied in low density, CERC plasmas but not yet under ion-root<sup>20</sup> and/or high density, high performance conditions.<sup>26,43</sup> Especially the latter ones exhibit an improved energy confinement for centrally peaked density profiles that are expected to also impact the impurity confinement. Here, future experiments need to show the  $Z$  dependent transport under suppressed anomalous transport conditions, especially with respect to impurity accumulation scenarios on the envisaged experiment program time scales of several minutes.

## ACKNOWLEDGMENTS

This work has been carried out within the framework of the EUROfusion Consortium and has received funding from the Euratom research and training programmes 2014–2018 and 2019–2020 under Grant Agreement No. 633053. The views and opinions expressed herein do not necessarily reflect those of the European Commission.

This scientific work was also partly supported by the Polish Ministry of Science and Higher Education within the framework of the scientific financial resources in the years 2014–2020 allocated for the realization of the international co-financed project.

## REFERENCES

- <sup>1</sup>F. Effenberg, S. Brezinsek, Y. Feng, R. Knig, M. Krychowiak, M. Jakubowski, H. Niemann, V. Perseo, O. Schmitz, D. Zhang *et al.*, *Nucl. Fusion* **59**, 106020 (2019).
- <sup>2</sup>D. Zhang, R. König, Y. Feng, R. Burhenn, S. Brezinsek, M. Jakubowski, B. Buttenschön, H. Niemann, A. Pavone, M. Krychowiak *et al.*, *Phys. Rev. Lett.* **123**, 025002 (2019).
- <sup>3</sup>A. Kallenbach, M. Balden, R. Dux, T. Eich, C. Giroud, A. Huber, G. Maddison, M. Mayer, K. McCormick, R. Neu *et al.*, in Proceedings of the 19th International Conference on Plasma-Surface Interactions in Controlled Fusion [J. Nucl. Mater. **415**, S19 (2011)].
- <sup>4</sup>A. Dinklage, K. McCarthy, C. Suzuki, N. Tamura, T. Wegner, H. Yamada, J. Balduhn, K. Brunner, B. Buttenschön, H. Damm *et al.*, *Nucl. Fusion* **59**, 076010 (2019).
- <sup>5</sup>R. Burhenn, Y. Feng, K. Ida, H. Maassberg, K. McCarthy, D. Kalinina, M. Kobayashi, S. Morita, Y. Nakamura, H. Nozato *et al.*, *Nucl. Fusion* **49**, 065005 (2009).
- <sup>6</sup>Y. Nakamura, N. Tamura, M. Yoshinuma, C. Suzuki, S. Yoshimura, M. Kobayashi, M. Yokoyama, M. Nunami, M. Nakata, K. Nagaoka *et al.*, *Nucl. Fusion* **57**, 056003 (2017).
- <sup>7</sup>T. S. Pedersen, R. Knig, M. Jakubowski, M. Krychowiak, D. Gradic, C. Killer, H. Niemann, T. Szepesi, U. Wenzel, A. Ali *et al.*, *Nucl. Fusion* **59**, 106020 (2019).
- <sup>8</sup>C. P. Dhard, M. Mayer, S. Brezinsek, S. Masuzaki, G. Motojima, R. Knig, T. S. Pedersen, R. Neu, D. Hathiramani, M. Krause *et al.*, *Fusion Eng. Des.* **146**, 242 (2019).
- <sup>9</sup>M. Tokitani, S. Masuzaki, and T. Murase, *Nucl. Mater. Energy* **18**, 23 (2019).
- <sup>10</sup>J. Rice, M. Reinke, C. Gao, N. Howard, M. Chilenski, L. Delgado-Aparicio, R. Granetz, M. Greenwald, A. Hubbard, J. Hughes *et al.*, *Nucl. Fusion* **55**, 033014 (2015).
- <sup>11</sup>M. Mattioli, C. D. Michelis, and A. Pecquet, *Nucl. Fusion* **38**, 1629 (1998).
- <sup>12</sup>M. Mattioli, R. Giannella, R. Myrnas, C. Demichelis, B. Denne-Hinnov, T. D. Wit, and G. Magyar, *Nucl. Fusion* **35**, 1115 (1995).
- <sup>13</sup>R. Giannella, L. Lauro-Taroni, M. Mattioli, B. Alper, B. Denne-Hinnov, G. Magyar, J. O. Rourke, and D. Pasini, *Nucl. Fusion* **34**, 1185 (1994).
- <sup>14</sup>D. Pasini, R. Giannella, L. L. Taroni, M. Mattioli, B. Denne-Hinnov, N. Hawkes, G. Magyar, and H. Weisen, *Plasma Phys. Controlled Fusion* **34**, 677 (1992).
- <sup>15</sup>A. Langenberg, N. A. Pablant, T. Wegner, P. Traverso, O. Marchuk, T. Bruer, B. Geiger, G. Fuchert, S. Bozhenkov, E. Pasch *et al.*, *Rev. Sci. Instrum.* **89**, 10G101 (2018).
- <sup>16</sup>S. Buller, H. M. Smith, P. Helander, A. Mollen, S. L. Newton, and I. Pusztai, *J. Plasma Phys.* **84**, 905840409 (2018).
- <sup>17</sup>C. Beidler, K. Allmaier, M. Isaev, S. Kasilov, W. Kernbichler, G. Leitold, H. Maaßberg, D. Mikkelsen, S. Murakami, M. Schmidt *et al.*, *Nucl. Fusion* **51**, 076001 (2011).
- <sup>18</sup>P. Helander and A. Zocco, *Plasma Phys. Controlled Fusion* **60**, 084006 (2018).
- <sup>19</sup>P. Helander, S. L. Newton, A. Mollén, and H. M. Smith, *Phys. Rev. Lett.* **118**, 155002 (2017).
- <sup>20</sup>N. A. Pablant, A. Langenberg, A. Alonso, C. D. Beidler, M. Bitter, S. Bozhenkov, R. Burhenn, M. Beurskens, L. Delgado-Aparicio, A. Dinklage *et al.*, *Phys. Plasmas* **25**, 022508 (2018).
- <sup>21</sup>J. M. García-Regaña, T. Estrada, I. Calvo, J. L. Velasco, J. A. Alonso, D. Carralero, R. Kleiber, M. Landreman, A. Mollén, E. Sánchez, and C. Slaby, *Plasma Phys. Controlled Fusion* **60**, 104002 (2018).
- <sup>22</sup>T. Wegner, B. Geiger, F. Kunkel, R. Burhenn, T. Schröder, C. Biedermann, B. Buttenschön, G. Cseh, P. Drews, O. Grulke *et al.*, *Rev. Sci. Instrum.* **89**, 073505 (2018).
- <sup>23</sup>A. Langenberg, F. Warmer, G. Fuchert, O. Marchuk, A. Dinklage, T. Wegner, J. A. Alonso, S. Bozhenkov, K. J. Brunner, R. Burhenn *et al.*, *Plasma Phys. Controlled Fusion* **61**, 014030 (2019).
- <sup>24</sup>J. Nührenberg, W. Lotz, P. Merkel, C. Nührenberg, U. Schwenn, E. Strumberger, and T. Hayashi, *Fusion Technol.* **27**, 71 (1995).
- <sup>25</sup>M. Kubkowska, A. Czarnecka, T. Fornal, M. Gruca, S. Jaboski, N. Krawczyk, L. Ry, R. Burhenn, B. Buttenschön, B. Geiger *et al.*, *Rev. Sci. Instrum.* **89**, 10F111 (2018).
- <sup>26</sup>R. C. Wolf, A. Alonso, S. Kslompolo, J. Balduhn, M. Beurskens, C. D. Beidler, C. Biedermann, H.-S. Bosch, S. Bozhenkov, R. Brakel *et al.*, *Phys. Plasmas* **26**, 082504 (2019).
- <sup>27</sup>T. Andreeva, “Vacuum magnetic configurations of Wendelstein 7-x,” Technical Report No. IPP III/270 (Max-Planck-Institut für Plasmaphysik, Garching, 2002).
- <sup>28</sup>R. C. Wolf, S. Bozhenkov, A. Dinklage, G. Fuchert, Y. O. Kazakov, H. P. Laqua, S. Marsen, N. B. Marushchenko, T. Stange, M. Zanini *et al.*, *Plasma Phys. Controlled Fusion* **61**, 014037 (2019).
- <sup>29</sup>G. Fussmann, *Nucl. Fusion* **26**, 983 (1986).
- <sup>30</sup>A. Langenberg, N. Pablant, O. Marchuk, D. Zhang, J. Alonso, R. Burhenn, J. Svensson, P. Valson, D. Gates, M. Beurskens *et al.*, *Nucl. Fusion* **57**, 086013 (2017).
- <sup>31</sup>A. Langenberg, J. Svensson, O. Marchuk, G. Fuchert, S. Bozhenkov, H. Damm, E. Pasch, A. Pavone, H. Thomsen, N. A. Pablant *et al.*, *Rev. Sci. Instrum.* **90**, 063505 (2019).
- <sup>32</sup>R. Bussiahn, N. Tamura, K. J. McCarthy, R. Burhenn, H. Hayashi, R. Laube, and T. Klinger, *Rev. Sci. Instrum.* **89**, 10K112 (2018).
- <sup>33</sup>M. Kubkowska, N. Tamura, A. Chomiczewska, T. Fornal, M. Gruca, N. Krawczyk, S. Jablonski, L. Ryc, R. Bussiahn, K.-J. Brunner *et al.*, *J. Instrum.* **15**, C01019 (2020).
- <sup>34</sup>R. Dux, “STRAHL user manual,” IPP Report No. 10/30 (Max-Planck-Institute for Plasma Physics, 2006).
- <sup>35</sup>S. P. Hirshman, K. C. Shaing, W. I. van Rij, C. O. Beasley, and E. C. Crume, *Phys. Fluids* **29**, 2951 (1986).
- <sup>36</sup>W. I. van Rij and S. P. Hirshman, *Phys. Fluids B* **1**, 563 (1989).
- <sup>37</sup>M. Landreman, H. M. Smith, A. Mollén, and P. Helander, *Phys. Plasmas* **21**, 042503 (2014).
- <sup>38</sup>A. Mollén, M. Landreman, and H. M. Smith, *J. Phys.* **561**, 012012 (2014).
- <sup>39</sup>A. Mollén, M. Landreman, H. M. Smith, J. M. García-Regaña, and M. Nunami, *Plasma Phys. Controlled Fusion* **60**, 084001 (2018).

- <sup>40</sup>B. Geiger, T. Wegner, C. Beidler, R. Burhenn, B. Buttenschn, R. Dux, A. Langenberg, N. Pablant, T. Pterich, Y. Turkin *et al.*, *Nucl. Fusion* **59**, 046009 (2019).
- <sup>41</sup>Y. Turkin, C. D. Beidler, H. Maassberg, S. Murakami, V. Tribaldos, and A. Wakasa, *Phys. Plasmas* **18**, 022505 (2011).
- <sup>42</sup>T. Wegner, B. Geiger, J. A. Alcuson, P. Xanthopoulos, R. Burhenn, F. Kunkel, C. Agnioni, M. Beurskens, L.-G. Böttger, S. Bozhenkov *et al.*, “Impact of the temperature ratio on turbulent impurity transport in Wendelstein 7-X,” *Phys. Rev. Lett.* (submitted).
- <sup>43</sup>S. A. Bozhenkov, Y. Kazakov, O. Ford, M. N. A. Beurskens, J. A. Alcuson, J. A. Alonso, J. Baldzuhn, C. Brandt, K. J. Brunner, H. Damm *et al.*, “High-performance plasmas after pellet injections in Wendelstein 7-X,” *Nucl. Fusion* (to be published) (2020).